

Harnessing the Power of Foundation Models for Accurate Material Classification

Qingran Lin^{1*} Fengwei Yang^{2*} Chaolun Zhu³

¹ Georgia Institute of Technology ² Duke University ³ Waseda University

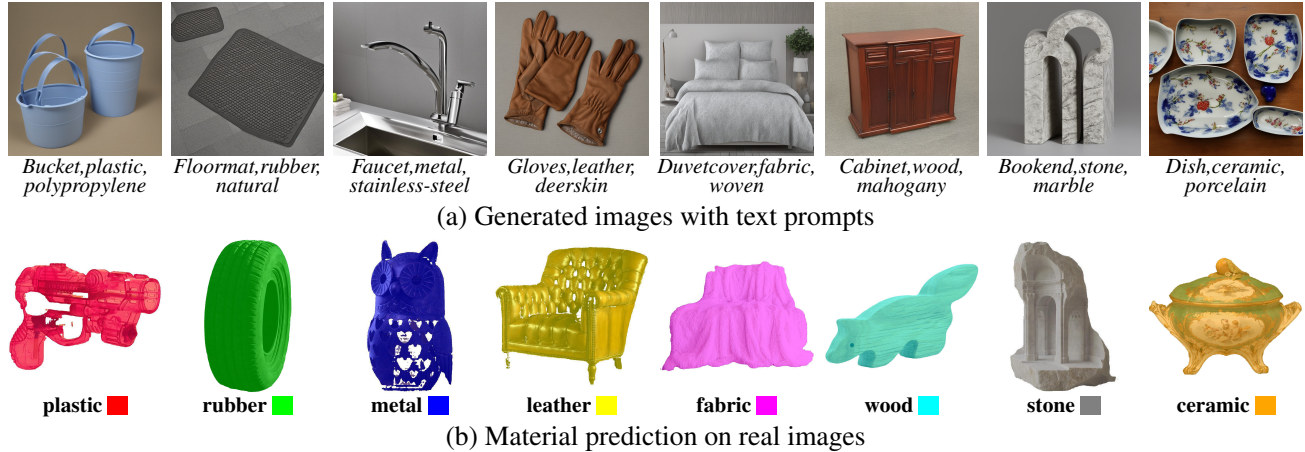


Figure 1. With careful knowledge distillation from image generation network, we built generated image material dataset and propose an method for accurate material classification

Abstract

Material classification has emerged as a critical task in computer vision and graphics, supporting the assignment of accurate material properties to a wide range of digital and real-world applications. While traditionally framed as an image classification task, this domain faces significant challenges due to the scarcity of annotated data, limiting the accuracy and generalizability of trained models. Recent advances in vision-language foundation models (VLMs) offer promising avenues to address these issues, yet existing solutions leveraging these models still exhibit unsatisfying results in material recognition tasks. In this work, we propose a novel framework that effectively harnesses foundation models to overcome data limitations and enhance classification accuracy. Our method integrates two key innovations: (a) a robust image generation and auto-labeling pipeline that creates a diverse and high-quality training dataset with material-centric images, and automatically assigns labels by fusing object semantics and material attributes in text prompts; (b) a prior incorporation strategy to distill information from VLMs, combined with

a joint fine-tuning method that optimizes a pre-trained vision foundation model alongside VLM-derived priors, preserving broad generalizability while adapting to material-specific features. Extensive experiments demonstrate significant improvements on multiple datasets. We show that our synthetic dataset effectively captures the characteristics of real world materials, and the integration of priors from vision-language models significantly enhances the final performance. The source code and dataset will be released.

1. Introduction

Accurate material classification is a fundamental problem in visual understanding, bridging raw observations to actionable material properties that are critical for rendering, simulation, and content generation. Recent advances in material modeling span three key directions including texture-space synthesis [12, 13, 17, 42, 43], image-space editing [6, 16, 23, 34], and material-aware 3D generation [11, 20, 41]. However, these workflows critically depend on robust material classification to map observations to actionable material parameters. For example, [41] leverage image-based classification to retrieve optimal procedu-

* Equal contribution.

ral materials from a database, underscoring its foundational role. Yet, despite material classification being framed as an image recognition task, existing solutions trained on limited annotated data struggle with reasonable distinctions (e.g., non-metallic vs. metallic surfaces). Even state-of-the-art vision-language models (VLMs) such as CLIP [29] or GPT-4v [1] pre-trained on web-scale data, exhibit a significant drop in material recognition accuracy compared to object classification, revealing a critical gap in domain-specific understanding. We attribute this to two factors: (1) the scarcity of high-quality, material-focused annotations for training, and (2) the underutilization of cross-modal priors in VLMs during training.

To address the scarcity of annotated material data, we propose synthesizing a labeled dataset using generative models. While modern diffusion-based methods [30, 32] can produce realistic images at scale, naively generating images with material prompts introduces two critical issues:

- **Material Ambiguity:** Generated images often depict *incorrect material correlations*—e.g., a foreground object labeled “ceramic” may appear alongside conflicting materials in the background (wooden tables, fabric textures).
- **Diversity Limitations:** Prompt engineering alone fails to ensure sufficient visual variation (lighting, viewpoints, occlusions), leading to poor generalization on real-world images.

To resolve these challenges, we introduce semantic grounding to enforce precise material-to-region associations. By augmenting generation prompts with *object semantics* and leveraging zero-shot segmentation models [21, 31], we isolate the target object (vase) and propagate its material label (ceramic) while filtering out irrelevant regions (marble table). This approach not only ensures auto-labeled accuracy but also enriches diversity by decoupling material from scene context. Through this design, we overcome the challenges of ambiguity and diversity in generative data, and produce a large-scale, auto-labeled dataset encompassing 21 material classes.

To harness cross-modal priors for improved generalization, we design a dual-stream framework that synergizes vision-based and language-based material representations. For visual grounding, we extract dense patch-level features using DINOv2 [27], a vision foundation model pretrained on unlabeled images, which captures fine-grained texture and reflectance patterns critical for material recognition. Simultaneously, we generate language descriptors of material appearance (e.g., “a glossy, translucent plastic with faint subsurface scattering”) using GPT-4v [1], then encode these textual descriptions into semantic embeddings via CLIP [29]. Crucially, this language stream distills domain-agnostic knowledge about material properties that may not be explicitly discernible from visual features alone. The two modalities are fused through a lightweight Multi-

layer Perceptron (MLP): DINOv2’s masked object features (aggregated via spatial averaging) are concatenated with CLIP’s language embeddings, then projected into a joint latent space for material prediction. This design ensures that visual cues are contextualized by semantic priors, enabling the model to disambiguate perceptually similar materials that can be identified from semantics. We finetune the head of DINOv2 together with the MLP during supervised training on our synthetic dataset to harness cross-modal priors while preserving the generalizability of both foundation models.

We validate our method on three datasets: the FMD [33] dataset, a classic 10-class benchmark for material classification; a 21-class DMS-test dataset constructed from the DMS [37] dataset; and a 21-class self-collected Google-test dataset from Google Images capturing real-world material appearances. Our approach achieves 89% accuracy on FMD [33] dataset and 92% on the Google-test dataset, outperforming state-of-the-art material classifier [9] by 33% and 29%, respectively. Notably, off-the-shelf vision-language models (VLMs) like CLIP [29] and GPT-4v [1] achieve only 38% and 43% accuracy on DMS-test dataset, highlighting their inadequacy for domain-specific tasks. Ablation results highlight the importance of both modalities, with the absence of language priors (GPT-4v + CLIP) reducing accuracy by at most 4%, and the removal of vision priors (DINOv2) causing a similar maximum drop. Crucially, models trained on our synthetic dataset outperform the DMS-trained baselines by 9% on the FMD [33] dataset and by 18% on the Google-test dataset. These results underscore the effectiveness of our unified solution in bridging synthetic dataset for real-world material recognition.

Overall, our core research contributions are:

- A synthetic data generation and auto-labeling framework for material classification that creates diverse, high-fidelity images with reliable labels, addressing the scarcity of annotated material data.
- A dual-stream framework for cross-modal prior fusion that combines vision-language and vision foundation models to improve generalizability and disambiguate perceptually similar materials.
- A collaborative fine-tuning strategy that preserves foundational model priors while adapting to material-specific tasks, achieving state-of-the-art performance on multiple datasets.

2. Related Work

Material datasets Material classification models are typically trained on datasets with annotated material images. Notable examples include FMD [33], which features 10 material categories, and OpenSurface [2], providing 19,000 indoor scene images covering 37 materials. MINC [3]

is larger, with 0.4 million images of 23 materials, while DMS [37] offers the most extensive collection, with 3.2 million segments in 44,560 images across 52 material classes. However, datasets such as OpenSurfaces [2] and DMS [37] exhibit a noticeable class imbalance, where common materials like wood and metal appear far more frequently than rare ones (e.g., wax, rubber). This unbalanced distribution hinders the model’s ability to generalize across diverse material types. [37]. To alleviate this issue, our generative dataset produces balanced samples across material categories, enabling more uniform and comprehensive supervision. Datasets like the Light-Field Material Dataset [38] and Multi-Illumination dataset [25], which account for varied lighting, are primarily designed for material parameter reconstruction rather than broad classification tasks due to their limited scale.

Generative dataset As text-to-image generation methods advance, there is a growing body of research leveraging these techniques to create datasets for learning purposes [10, 26, 36]. We follow this approach to generate our material image dataset, with a focus on overcoming specific challenges such as maintaining content diversity and ensuring automatic and accurate material labeling.

Material recognition Material recognition research has focused on classification, with key developments including the FV-CNN technique by Cimpoi et al. [7], which combines CNNs with IFV classifiers and has been tested on datasets like OpenSurfaces [2] and FMD [33]. Recently, [4] introduced the KITTI-Materials dataset and RMSNet, a hierarchical Transformer-based model for road scene material segmentation using RGB images. Mei et al. [24] presented PGSNet, which uses RGB and polarization data to segment glass materials, outperforming previous models on the RGBP-Glass dataset. Manuel et al. [9] developed a contractive learning method for material classification trained on MatSim, a dataset which incorporates synthetic physical rendering images and natural images. Their approach rivals CLIP [29] in general material classification. Recently, advancements in vision backbones have led to the development of more effective architectures for image classification, such as ConvNeXt [39], HRNet [35], Vision Transformer (ViT) [8], Swim-T [22], and Masked Autoencoders (MAE) [15]. Despite these advances, there is room for improvement in the generalization capabilities of these methods. Our goal is to integrate the latest unsupervised vision models [27] with our extensive synthetic dataset, created using foundational vision models, to enhance generalizability and achieve precise material classification for real-world images.

Harness Foundation Models for Vision Tasks Recent works leverage foundation models for vision tasks through two paradigms: vision-only priors and vision-language alignment. For vision-centric learning, methods like DINOv2 [27] exploit self-supervised pretraining to extract generalizable features for segmentation. [40] and [18] further exploit such generalizable features for depth and PBR parameter estimation. However, such approaches struggle with generalizability for material classification due to the sparsity of data. Concurrently, vision-language models (VLMs) like CLIP [29] and GPT-4v [1] enable zero-shot material classification in works such as MAPA [41] and Make-It-Real [11], which align material descriptors with images. While these methods bypass manual annotation, they exhibit limited accuracy on fine-grained materials due to (1) vague text prompts that fail to capture nuanced visual properties and (2) inadequate adaptation to small, domain-specific datasets. Instead, we finetune a dual-stream network architecture to better exploit both language and vision priors.

3. Method

Our framework addresses material classification through two synergistic components: (1) synthetic dataset generation with semantic-aware auto-labeling to overcome annotation scarcity, and (2) a dual-stream architecture that fuses vision-language priors for robust feature learning. For synthetic data generation (Section 3.1), we first mitigate data limitations by generating a diverse material-centric dataset using text-to-image diffusion models. The pipeline integrates object-aware prompt engineering with vision foundation models (DINOv2, Grounding DINO) for automatic region-material labeling. For learning material classification, we formulate the material classification as a cross-modal fusion task with both vision and language streams in Sections 3.2. Finally, we present our dual-stream network architecture along with the training specifics in Section 3.3.

3.1. Synthetic Dataset

Our synthetic dataset generation process addresses annotation scarcity by combining hierarchical prompt engineering, material image generation, and automated label validation. The workflow (Fig. 2) ensures high-quality material-image associations while maximizing diversity.

Prompt Design with Validation To generate plausible object-material pairs, we employ a three-tiered prompting strategy: *object*, *material category* (wood, metal, plastic, etc.), and *sub-material* (e.g., “stainless steel” under “metal”) or an *adjective* describing the material (e.g., “polished” metal).. We first instruct ChatGPT to produce candidate triplets (e.g., “vase, ceramic, porcelain”), filtering

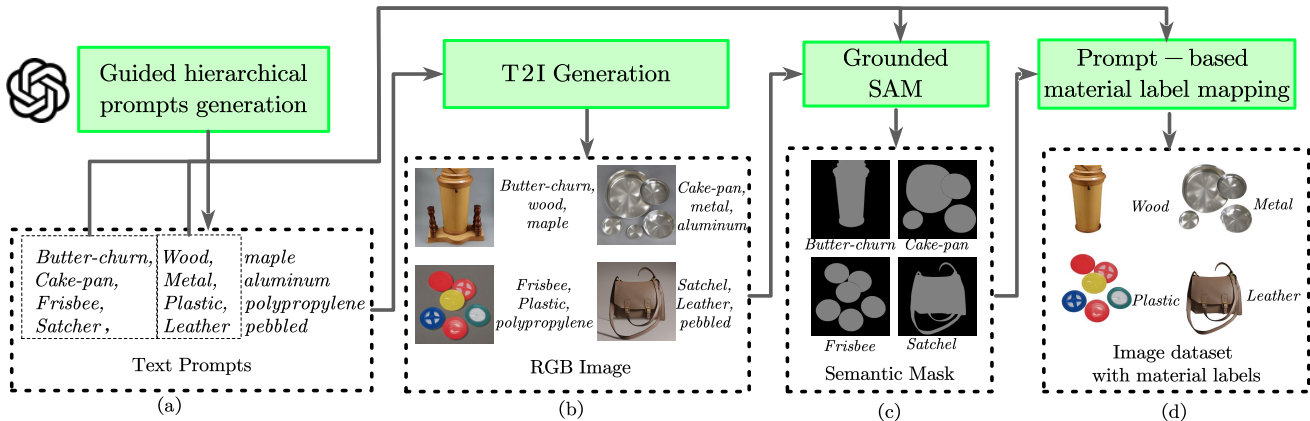


Figure 2. Dataset generation workflow. Our pipeline synthesizes labeled material images through: (a) Hierarchical prompt engineering with LLM-guided plausibility filtering, (b) Diffusion-based image generation with model selection, (c) Semantic mask extraction, and (d) Region-aware material label assignment.



Figure 3. Generated material images using diverse prompts across 21 material categories, with one image per category.

implausible combinations (e.g., “sponge, metal”) via human validation. By discarding implausible combinations, this step ensures both realism and diversity in the generated pairings. Compared to free-form prompting or attribute lists (e.g., “a wooden object”), our approach improves text-to-image alignment since we can further perform semantic segmentation to align material and related image region.

Material Image Generation We qualitatively evaluate four diffusion models—SDXL [28], Stable Diffusion v2.1 [32], PixArt- α [5] and Playground v2.5 [19] to assess the fidelity and diversity of generated material images. Through the inspection of generated images we find SDXL produces images with marginally higher visual quality than SD v2.1 but introduces subtle artifacts in texture patterns

(e.g. unrealistic wood grain). PixArt- α and Playground v2.5 exhibit superior artistic styling compared to SDXL, yet they share similar issues concerning texture realism. Given these findings, we select SDv2.1 for its balance of material accuracy and diversity, synthesizing 20k+ images across 21 categories: plastic, metal, leather, fabric, wood, stone, ceramic, water, sponge, bone, cardboard, concrete, foliage, fur, gemstone, glass, paper, soil, wax, wicker, rubber, thus offering broad coverage of real-world materials. As depicted in Figure 3, the generated images closely align with the prompts, and their quality is commendable.

Auto-Labeling via Semantic Grounding To resolve material ambiguity in generated scenes (e.g., a “ceramic vase” on a “wooden table”), we apply Grounding DINO [21]

to segment the target object using the *object* field from prompts. Material labels are assigned exclusively to the segmented region, filtering out conflicting materials in background areas. This approach achieves 98% label accuracy on human-verified samples, which is hard to achieve based on pure material recognition, but reversely can be used to create a dataset that is helpful for improving material recognition.

Automatic material labeling. We’ve observed that diffusion models often produce images featuring multiple material categories, with the associated material typically appearing as the primary object or a significant part of the image. This can significantly impair learning performance if the entire image and its material label are used directly for training. A more substantial challenge is the absence of a method to directly identify the correct material regions, as this is the core problem we aim to solve. However, we’ve discovered an effective solution to this issue by employing semantic labels as a mediator. As shown in Figure 2 (c), we use Grounded SAM [31] to incorporate object semantics from the text prompt as input to detect and segment the object areas within the image. For instance, if the text prompt is “Cake-pan”, Grounded SAM can identify and segment the Cake-pan within the image. Since material and semantic features are usually accurately combined during the generation process, and semantic understanding solutions are well-established, we can label the material areas in the image with high precision through prompt-based material label mapping in Figure 2 (d). This approach allows us to address the challenge of material region identification and enhance the accuracy of our material classification model.

3.2. Formulation

Given an image \mathcal{I} and a binary mask \mathcal{M} denoting the region of interest, we predict the material label l by fusing *vision* and *language* foundation model priors. Let \mathcal{T} represent a text descriptor of material properties (e.g., “porous ceramic with matte finish”) generated offline for each class. The prediction is formulated as:

$$l = \mathcal{C}(\mathcal{E}_{\text{vis}}(\mathcal{I}, \mathcal{M}), \mathcal{E}_{\text{txt}}(\mathcal{T})),$$

where \mathcal{E}_{vis} extracts visual features from the masked region and \mathcal{E}_{txt} encodes textual material descriptors.

Vision Prior Stream extracts dense features using a frozen vision foundation model ϕ_{vis} :

$$\mathbf{f}_{\text{vis}} = \mathcal{A}_{\text{vis}}(\phi_{\text{vis}}(\mathcal{I}) \circ \mathcal{M}),$$

where \circ denotes element-wise masking and $\mathcal{A}_{\text{vis}} : \mathbb{R}^{H' \times W' \times D} \rightarrow \mathbb{R}^{d_{\text{vis}}}$ aggregates features (e.g., masked average pooling).

Language Prior Stream encodes material semantics using a frozen VLM ϕ_{txt} :

$$\mathbf{f}_{\text{txt}} = \mathcal{A}_{\text{txt}}(\phi_{\text{txt}}(\mathcal{T})),$$

where $\mathcal{A}_{\text{txt}} : \mathbb{R}^{D_{\text{txt}}} \rightarrow \mathbb{R}^{d_{\text{txt}}}$ projects text embeddings to a latent space.

Cross-Modal Fusion combines both streams via:

$$l = \underset{k}{\operatorname{argmax}}(\operatorname{MLP}(\mathbf{f}_{\text{vis}} \oplus \mathbf{f}_{\text{txt}})),$$

where \oplus denotes concatenation. The model is trained using cross-entropy loss:

$$\mathcal{L} = - \sum_{k=1}^K \hat{l}_k \log p_k,$$

where p_k is the predicted probability for class k and \hat{l}_k the ground truth label. Frozen ϕ_{vis} and ϕ_{txt} preserve pre-trained priors while \mathcal{A}_{vis} , \mathcal{A}_{txt} , and MLP are learnable.

3.3. Network Architecture

Our dual-stream architecture combines vision foundation model features with language-guided material semantics (Figure . 4).

Vision Stream employs DINOv2 [27] as the backbone encoder \mathcal{E}_{vis} . For an input image \mathcal{I} , it produces dense patch features:

$$\{\mathbf{f}_{(i,j)}\} = \mathcal{E}_{\text{DINOv2}}(\mathcal{I}) \in \mathbb{R}^{32 \times 32 \times 768},$$

where each $\mathbf{f}_{(i,j)}$ corresponds to a 32×32 image patch. We downsample the binary mask \mathcal{M} to 32×32 resolution, retaining only features where $\mathcal{M}_{(i,j)} > 0$. These masked features are aggregated via max-pooling:

$$\mathbf{f}_{\text{vis}} = \max_{i,j}(\{\mathbf{f}_{(i,j)}\} \circ \mathcal{M}) \in \mathbb{R}^{768}.$$

Language Stream encodes material semantics using CLIP [29]. For each image to recognize, we ask GPT-4V [1] to generate descriptive text \mathcal{T}_k (e.g., “appears polished and shines with reflections ...” shown in Figure 4). CLIP’s text encoder ϕ_{txt} projects these into embeddings:

$$\mathbf{f}_{\text{txt}}^k = \phi_{\text{txt}}(\mathcal{T}_k) \in \mathbb{R}^{512}.$$

During training, we use the ground truth class embedding \mathbf{f}_{txt} ; at inference, all class embeddings are compared.

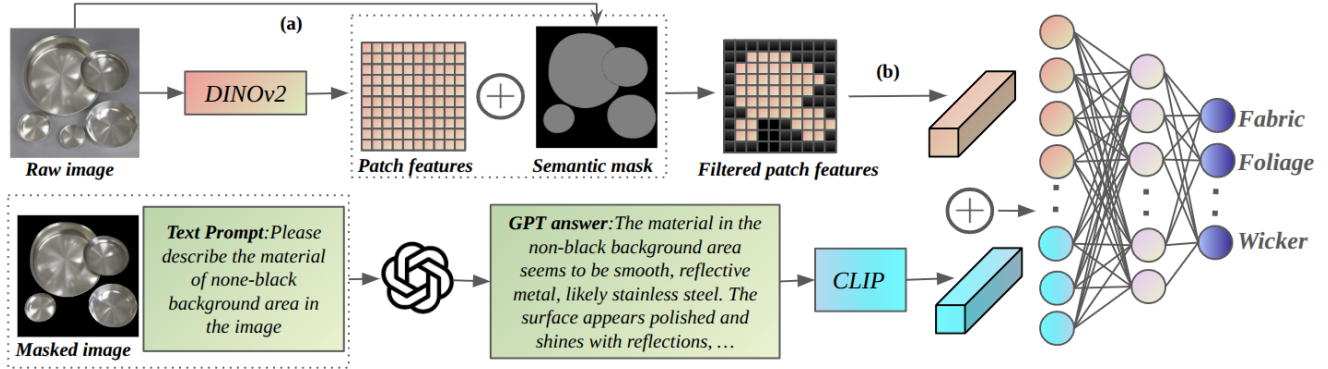


Figure 4. Dual-stream architecture. (1) **Vision Stream**: DINOv2 extracts patch features from the masked region, aggregated via max-pooling. (2) **Language Stream**: GPT-4v generates material descriptors encoded by CLIP. The fused features are classified via MLP. (a) Grounded SAM semantic mask extraction (b) Feature aggregation (max-pooling + flatten)

Fusion & Classification concatenates both modalities:

$$\mathbf{f}_{\text{fuse}} = \mathbf{f}_{\text{vis}} \oplus \mathbf{f}_{\text{txt}} \in \mathbb{R}^{768+512},$$

where \oplus denotes concatenation. A MLP maps \mathbf{f}_{fuse} to class probabilities:

$$p(l = k) = \text{MLP}(\mathbf{f}_{\text{fuse}})_k.$$

Training Protocol We freeze DINOv2 and CLIP to preserve pretrained priors and train only MLP parameters with AdamW (lr=5e-5). This ensures adaptation to material recognition without catastrophic forgetting of foundation model knowledge.

4. Experiment

4.1. Overview

We evaluate both the proposed material classification method and the quality of the datasets as our core contributions. In our experiments, we evaluate performance using mean Intersection over Union (mIoU) following the protocol in [37] and mean Accuracy (mAcc). For methods involving GPT-4v, however, we report accuracy only. In Section 4.2, we compare our method with state-of-the-art methods to demonstrate its effectiveness. To ensure a fair comparison, we conduct experiments on three datasets: the FMD [33] dataset, a classic 10-class benchmark for material classification; the DMS-test dataset, a 21-class subset we constructed from the comprehensive DMS [37] dataset; and the Google-test dataset, a curated 21-class collection from Google Images that provides higher-quality samples and better reflects real-world material appearances as well as artist-created content. To evaluate the quality of our synthetic dataset relative to the public DMS [37] dataset, we train our vision module separately on two datasets and compare the material classification performance on DMS-test, Google-test and FMD [33]. In Section 4.3, we further

conduct ablation studies to investigate the contributions of each component of our proposed method. This includes the dual-stream language and vision architecture, the selection of the vision backbone, and the impact of dataset scale and with/without auto labeled semantics on our task.

4.2. Comparison

Compare with SOTA methods Due to the scarcity of high-quality data in material classification tasks, recent state-of-the-art methods, such as Mapa [41] and Make-It-Real [11], have begun to incorporate priors from zero-shot foundation models, notably CLIP [29] and GPT-4v [1], for material segmentation purposes. In our study, we compare our proposed approach against these models.

For CLIP, we adopt the ViT-H/14 model, which was trained on approximately two billion image-text pairs, to serve as a strong baseline for comparison. We first use CLIP [29] to encode the candidate material texts (plastic, foliage, glass etc.) and the input test image. We then select the material text whose encoded feature is the nearest neighbor to the feature encoded by the input image as the predicted material. For evaluation, we consider 10 classes that align with FMD [33], whereas for DMS-test and Google-test we use the full set of 21 classes. For GPT-4v [1], we evaluate its performance by prompting it with “Please identify the material of the non-masked area.” A prediction is regarded as correct if the response contains the ground-truth class label of the input image.

In addition to comparing with zero-shot foundation models, we also evaluate our approach against baselines and the state-of-the-art method proposed in MatSim [9] for general material classification. The MatSim method outputs a 512-dimensional descriptive vector for each region. To assess its performance, we follow this procedure: each image in the test dataset is matched against all other images based on the similarity of their feature vectors. If the best-matched image belongs to the same class, it is considered correctly

classified.

The comparison results are shown in Table 1 (Material classification performance on the FMD [33] dataset) and Table 2 (Material classification performance on the DMS-test dataset and Google test dataset). Our approach significantly outperforms both zero-shot CLIP [29] and zero-shot GPT-4v [1]. This result indicates that zero-shot foundation models struggle with material classification, likely due to limited exposure to labeled material data during training. Furthermore, our approach significantly outperforms MatSim [9], a state-of-the-art method specifically designed for material tasks. This advantage is likely due to our innovative dual-stream architecture and higher-quality training data. These results highlight the substantial superiority of our approach over existing methods.

Table 1. Comparison with state-of-the-art methods on the FMD dataset (10 classes). All values denote classification accuracy (truncated to two decimal places), and the best result in each row is highlighted in **bold**.

Method \ Class	CLIP[29]	GPT-4v [1]	MatSim[9]	Ours
fabric	0.66	0.85	0.47	1.00
foliage	0.93	0.19	0.82	0.97
glass	0.84	0.76	0.57	0.87
leather	0.67	0.87	0.57	0.85
metal	0.62	0.61	0.47	0.94
paper	0.83	0.88	0.39	0.84
plastic	0.90	0.87	0.52	0.90
stone	0.87	0.64	0.62	0.91
water	0.84	0.83	0.57	0.92
wood	0.91	0.95	0.62	0.75
Average	0.80	0.74	0.56	0.89

Table 2. Comparison of material classification on the DMS-test dataset (21 classes) and the Google-test dataset (21 classes). All values denote classification accuracy, and the best result in each row is highlighted in **bold**.

Method \ Dataset	CLIP[29]	GPT-4v [1]	MatSim [9]	Ours
DMS-test	0.38	0.43	0.41	0.64
Google-test	0.81	0.74	0.63	0.92

Analysis of dataset quality We evaluate the quality of our synthetic dataset by comparing it with the state-of-the-art (SOTA) dataset, DMS [37], which contains 3.2 million dense material segments and is currently the largest material segmentation dataset available. We train our vision branch(DINOv2) separately on DMS dataset and our synthetic dataset and compare the material classification performance on DMS-test, Google-test and FMD [33]. As expected, in-domain evaluation, where the model is trained on the DMS dataset and tested on DMS-test, achieves relatively higher performance compared to models trained on

our synthetic dataset. However, this advantage disappears in cross-dataset evaluation, and when tested on Google-test and FMD, the synthetic-trained model significantly outperforms the DMS-trained one as shown in Table 3. These results suggest that while DMS provides moderate in-domain performance, it lacks sufficient generalization ability. Figure 5 provides further insights by visualizing PCA distributions of ten material classes, derived from max-pooled aggregated DINOv2 patch features. The FMD samples (blue) form compact clusters with small intra-class variation. In contrast, the DMS samples (orange) appear more dispersed and often shifted from FMD, revealing a clear domain gap between the two datasets. This gap is reflected not only in the mean shift but also in differences in variance and distributional shape, indicating that the two datasets capture distinct feature statistics. Our synthetic samples (green) not only overlap with DMS but also align more closely with FMD, thereby bridging the two distributions. This explains why synthetic training achieves superior cross-domain performance, as the synthesis pipeline combining validated prompt design, material image generation, semantic grounding, and automatic annotation introduces greater diversity that extends the representational coverage beyond existing benchmark.

Table 3. Comparison on material classification with DMS dataset(mIoU|mAcc). Best in **bold**.

Train data \ Test data	DMS-test	Google-test	FMD [33]
DMS[37]	0.52 0.67	0.57 0.71	0.67 0.79
Ours	0.46 0.60	0.81 0.89	0.79 0.88

4.3. Ablation test

Ablation study of dual modules We evaluate the contributions of the language and vision streams in our network. To achieve this, we trained the vision stream (DINOv2) and the language stream (GPT-4v + CLIP) separately on our generated dataset and assessed their performance on three test datasets. As shown in Table 4, our proposed dual-stream method achieved the best performance on all test datasets in both mIoU and mAcc. This result validates the effectiveness of fusing language and vision priors in our approach.

Table 4. Influence of language (GPT-4v+CLIP) and vision (DINOv2) priors to the performance of material classification(mIoU|mAcc). Best in **bold**.

GPT-4v+CLIP	DINOv2	Google-test	DMS-test	FMD [33]
✓	×	0.83 0.90	0.49 0.64	0.74 0.85
×	✓	0.81 0.89	0.46 0.60	0.79 0.88
✓	✓	0.86 0.92	0.50 0.64	0.81 0.89

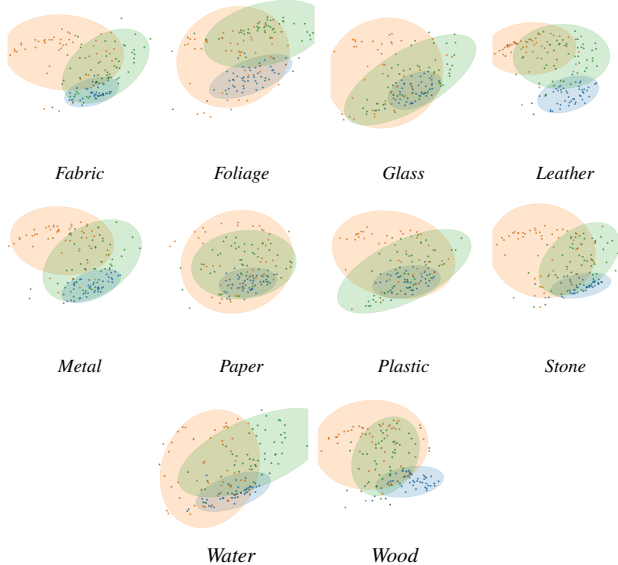


Figure 5. PCA overlays of max-pooled DINOv2 patch features from 10 material classes across FMD, DMS, and Ours datasets. Axes are fixed to $[-40, 40]$ on both dimensions. Each dataset is shown with scatter points and its covariance ellipse (two standard deviations), highlighting intra-class variation.

Compare across different vision backbones To analyze the impact of model capacity on the performance of the vision stream, we explored different vision backbone architectures by replacing our DINOv2 component with Vision Transformer (ViT) [8] and ResNet [14]. All models are trained on our generated dataset and evaluated on FMD [33]. We also investigated whether to release all parameters (full) or only the head parameters (head) for training. Table 5 shows that when training in “full” mode, the model with a ResNet backbone achieved the highest performance (0.44mIoU|0.61mAcc) among the tested models, while the model based on a DINOv2 backbone obtained the lowest score (0.23mIoU|0.38mAcc). This suggests that models with lighter parameter capacity perform better when trained in full mode. When training in “head” mode (i.e. only fine-tuning the MLP layer), our vision stream approach (DINOv2-head) achieved the best performance (0.79mIoU|0.88mAcc) among all tested models. This is likely due to the powerful pre-trained image features produced by DINOv2. In contrast, ResNet-head, which has the smallest backbone capacity, had the worst performance (0.48mIoU|0.64mAcc) among the models trained in “head” mode. In summary, we found that the DINOv2-head configuration performed the best and thus selected it as our vision backbone.

The influence of dataset scale To explore how dataset scale affects model performance, we trained our network

Table 5. Comparison of material classification performance across different vision backbones(mIoU|mAcc). Best in **bold**.

Train method	Vision backbone		
	ResNet-101	ViT-L/16	DINOv2
head	0.48 0.64	0.50 0.66	0.79 0.88
full	0.44 0.61	0.34 0.51	0.23 0.38

(using only the vision stream for simplicity) on datasets with varying numbers of images, and evaluated it on the FMD [33] dataset. The results are shown in Figure 6. The baseline (1x) corresponds to a dataset generated from 2448 prompts distributed across the 10 classes, with each prompt producing 5 images, resulting in a total of 12,240 images. As shown in Figure 6, both mIoU and mAcc increase rapidly when scaling from 0.2x to 1x, confirming the benefit of enlarging the training set in the low-data regime. Although performance gains plateau beyond 2x (0.80mIoU|0.89mAcc), this trend indicates that increasing the dataset scale consistently enhances performance, highlighting the promise of our generation pipeline for constructing larger datasets tailored to more complex material recognition tasks.

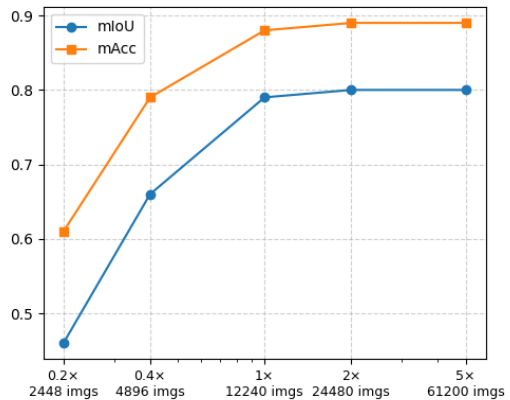


Figure 6. Model performance in relation to the number of images.

Comparison with/without auto labeled semantics We investigated the effect of auto-labeled semantics by comparing our approach against a variant without semantic labels, in which all image patches were directly max-pooled during training. To this end, we constructed a dataset with empty masks, trained the vision branch on it, and evaluated performance on FMD [33]. The auto-labeled model achieved (0.79mIoU|0.88mAcc), compared to (0.75mIoU|0.85mAcc) without semantic labels, corresponding to improvements of 4% in mIoU and 3% in mAcc.

5. Conclusion

We introduce a novel framework for material classification that addresses limited annotated data by leveraging

vision-language models and an auto-labeling pipeline. Our method enhances accuracy through joint fine-tuning and achieves superior performance across datasets. This work highlights the potential of synthetic data and VLM-guided priors for scalable material recognition.

References

- [1] Josh Achiam, Steven Adler, Sandhini Agarwal, Lama Ahmad, Ilge Akkaya, Florencia Leoni Aleman, Diogo Almeida, Janko Altenschmidt, Sam Altman, Shyamal Anadkat, et al. Gpt-4 technical report. *arXiv preprint arXiv:2303.08774*, 2023. 2, 3, 5, 6, 7, 1
- [2] Sean Bell, Paul Upchurch, Noah Snively, and Kavita Bala. Opensurfaces: A richly annotated catalog of surface appearance. *ACM TOG*, 32(4):1–17, 2013. 2, 3
- [3] Sean Bell, Paul Upchurch, Noah Snively, and Kavita Bala. Material recognition in the wild with the materials in context database. In *CVPR*, pages 3479–3487, 2015. 2
- [4] Sudong Cai, Ryosuke Wakaki, Shohei Nobuhara, and Ko Nishino. Rgb road scene material segmentation. In *ACCV*, pages 3051–3067, 2022. 3
- [5] Junsong Chen, Jincheng Yu, Chongjian Ge, Lewei Yao, Enze Xie, Yue Wu, Zhongdao Wang, James Kwok, Ping Luo, Huchuan Lu, et al. Pixart-*alpha*: Fast training of diffusion transformer for photorealistic text-to-image synthesis. *arXiv preprint arXiv:2310.00426*, 2023. 4
- [6] Ta-Ying Cheng, Prafull Sharma, Andrew Markham, Niki Trigoni, and Varun Jampani. Zest: Zero-shot material transfer from a single image. In *European Conference on Computer Vision*, pages 370–386. Springer, 2025. 1
- [7] Mircea Cimpoi, Subhansu Maji, and Andrea Vedaldi. Deep filter banks for texture recognition and segmentation. In *CVPR*, pages 3828–3836, 2015. 3
- [8] Alexey Dosovitskiy. An image is worth 16x16 words: Transformers for image recognition at scale. *arXiv preprint arXiv:2010.11929*, 2020. 3, 8
- [9] Manuel S Drehwald, Sagi Eppel, Jolina Li, Han Hao, and Alan Aspuru-Guzik. One-shot recognition of any material anywhere using contrastive learning with physics-based rendering. In *Proceedings of the IEEE/CVF International Conference on Computer Vision*, pages 23524–23533, 2023. 2, 3, 6, 7, 1
- [10] Lisa Dunlap, Alyssa Umino, Han Zhang, Jiezhi Yang, Joseph E Gonzalez, and Trevor Darrell. Diversify your vision datasets with automatic diffusion-based augmentation. *Advances in neural information processing systems*, 36:79024–79034, 2023. 3
- [11] Ye Fang, Zeyi Sun, Tong Wu, Jiaqi Wang, Ziwei Liu, Gordon Wetzstein, and Dahua Lin. Make-it-real: Unleashing large multimodal model’s ability for painting 3d objects with realistic materials. *arXiv preprint arXiv:2404.16829*, 2024. 1, 3, 6
- [12] Paul Guerrero, Miloš Hašan, Kalyan Sunkavalli, Radomír Měch, Tamy Boubekeur, and Niloy J Mitra. Matformer: A generative model for procedural materials. *arXiv preprint arXiv:2207.01044*, 2022. 1
- [13] Yu Guo, Cameron Smith, Miloš Hašan, Kalyan Sunkavalli, and Shuang Zhao. Materialgan: Reflectance capture using a generative svbrdf model. *arXiv preprint arXiv:2010.00114*, 2020. 1
- [14] Kaiming He, Xiangyu Zhang, Shaoqing Ren, and Jian Sun. Deep residual learning for image recognition. In *CVPR*, pages 770–778, 2016. 8
- [15] Kaiming He, Xinlei Chen, Saining Xie, Yanghao Li, Piotr Dollár, and Ross Girshick. Masked autoencoders are scalable vision learners. In *Proceedings of the IEEE/CVF conference on computer vision and pattern recognition*, pages 16000–16009, 2022. 3
- [16] Yiwei Hu, Miloš Hašan, Paul Guerrero, Holly Rushmeier, and Valentin Deschaintre. Controlling material appearance by examples. In *Computer graphics forum*, pages 117–128. Wiley Online Library, 2022. 1
- [17] Yiwei Hu, Paul Guerrero, Milos Hasan, Holly Rushmeier, and Valentin Deschaintre. Generating procedural materials from text or image prompts. In *ACM SIGGRAPH 2023 Conference Proceedings*, pages 1–11, 2023. 1
- [18] Xin Huang, Tengfei Wang, Ziwei Liu, and Qing Wang. Material anything: Generating materials for any 3d object via diffusion. *arXiv preprint arXiv:2411.15138*, 2024. 3
- [19] Daiqing Li, Aleks Kamko, Ehsan Akhgari, Ali Sabet, Linmiao Xu, and Suhail Doshi. Playground v2. 5: Three insights towards enhancing aesthetic quality in text-to-image generation. *arXiv preprint arXiv:2402.17245*, 2024. 4
- [20] Zeyu Li, Ruitong Gan, Chuanchen Luo, Yuxi Wang, Jiaheng Liu, Ziwei Zhu, Qing Li, Xucheng Yin, Man Zhang, Zhaoxiang Zhang, et al. Materialseg3d: Segmenting dense materials from 2d priors for 3d assets. In *Proceedings of the 32nd ACM International Conference on Multimedia*, pages 370–379, 2024. 1
- [21] Shilong Liu, Zhaoyang Zeng, Tianhe Ren, Feng Li, Hao Zhang, Jie Yang, Qing Jiang, Chunyuan Li, Jianwei Yang, Hang Su, et al. Grounding dino: Marrying dino with grounded pre-training for open-set object detection. *arXiv preprint arXiv:2303.05499*, 2023. 2, 4
- [22] Ze Liu, Yutong Lin, Yue Cao, Han Hu, Yixuan Wei, Zheng Zhang, Stephen Lin, and Baining Guo. Swin transformer: Hierarchical vision transformer using shifted windows. In *Proceedings of the IEEE/CVF international conference on computer vision*, pages 10012–10022, 2021. 3
- [23] Ivan Lopes, Fabio Pizzati, and Raoul de Charette. Material palette: Extraction of materials from a single image. In *Proceedings of the IEEE/CVF Conference on Computer Vision and Pattern Recognition*, pages 4379–4388, 2024. 1
- [24] Haiyang Mei, Bo Dong, Wen Dong, Jiayi Yang, Seung-Hwan Baek, Felix Heide, Pieter Peers, Xiaopeng Wei, and Xin Yang. Glass segmentation using intensity and spectral polarization cues. In *CVPR*, pages 12622–12631, 2022. 3
- [25] Lukas Murmann, Michael Gharbi, Miika Aittala, and Fredo Durand. A dataset of multi-illumination images in the wild. In *CVPR*, pages 4080–4089, 2019. 3
- [26] Quang Nguyen, Truong Vu, Anh Tran, and Khoi Nguyen. Dataset diffusion: Diffusion-based synthetic data generation for pixel-level semantic segmentation. *Advances in Neural Information Processing Systems*, 36, 2024. 3

- [27] Maxime Oquab, Timothée Darcet, Théo Moutakanni, Huy Vo, Marc Szafranec, Vasil Khalidov, Pierre Fernandez, Daniel Haziza, Francisco Massa, Alaaeldin El-Nouby, et al. Dinov2: Learning robust visual features without supervision. *arXiv preprint arXiv:2304.07193*, 2023. 2, 3, 5
- [28] Dustin Podell, Zion English, Kyle Lacey, Andreas Blattmann, Tim Dockhorn, Jonas Müller, Joe Penna, and Robin Rombach. Sdxl: Improving latent diffusion models for high-resolution image synthesis. *arXiv preprint arXiv:2307.01952*, 2023. 4
- [29] Alec Radford, Jong Wook Kim, Chris Hallacy, Aditya Ramesh, Gabriel Goh, Sandhini Agarwal, Girish Sastry, Amanda Askell, Pamela Mishkin, Jack Clark, et al. Learning transferable visual models from natural language supervision. In *International conference on machine learning*, pages 8748–8763. PMLR, 2021. 2, 3, 5, 6, 7, 1
- [30] Aditya Ramesh, Mikhail Pavlov, Gabriel Goh, Scott Gray, Chelsea Voss, Alec Radford, Mark Chen, and Ilya Sutskever. Zero-shot text-to-image generation. In *International conference on machine learning*, pages 8821–8831. Pmlr, 2021. 2
- [31] Tianhe Ren, Shilong Liu, Ailing Zeng, Jing Lin, Kunchang Li, He Cao, Jiayu Chen, Xinyu Huang, Yukang Chen, Feng Yan, et al. Grounded sam: Assembling open-world models for diverse visual tasks. *arXiv preprint arXiv:2401.14159*, 2024. 2, 5
- [32] Robin Rombach, Andreas Blattmann, Dominik Lorenz, Patrick Esser, and Björn Ommer. High-resolution image synthesis with latent diffusion models. In *Proceedings of the IEEE/CVF conference on computer vision and pattern recognition*, pages 10684–10695, 2022. 2, 4
- [33] Lavanya Sharan, Ruth Rosenholtz, and Edward H. Adelson. Accuracy and speed of material categorization in real-world images. *J. Vis.*, 14(10), 2014. 2, 3, 6, 7, 8
- [34] Prafull Sharma, Varun Jampani, Yuanzhen Li, Xuhui Jia, Dmitry Lagun, Fredo Durand, Bill Freeman, and Mark Matthews. Alchemist: Parametric control of material properties with diffusion models. In *Proceedings of the IEEE/CVF Conference on Computer Vision and Pattern Recognition*, pages 24130–24141, 2024. 1
- [35] Ke Sun, Yang Zhao, Borui Jiang, Tianheng Cheng, Bin Xiao, Dong Liu, Yadong Mu, Xinggang Wang, Wenyu Liu, and Jingdong Wang. High-resolution representations for labeling pixels and regions. *arXiv preprint arXiv:1904.04514*, 2019. 3
- [36] Aysim Toker, Marvin Eisenberger, Daniel Cremers, and Laura Leal-Taixé. Satsynth: Augmenting image-mask pairs through diffusion models for aerial semantic segmentation. In *Proceedings of the IEEE/CVF Conference on Computer Vision and Pattern Recognition*, pages 27695–27705, 2024. 3
- [37] Paul Upchurch and Ransen Niu. A dense material segmentation dataset for indoor and outdoor scene parsing. In *ECCV*, pages 450–466, 2022. 2, 3, 6, 7
- [38] Ting-Chun Wang, Jun-Yan Zhu, Ebi Hiroaki, Manmohan Chandraker, Alexei A Efros, and Ravi Ramamoorthi. A 4d light-field dataset and cnn architectures for material recognition. In *ECCV*, pages 121–138, 2016. 3
- [39] Sanghyun Woo, Shoubhik Debnath, Ronghang Hu, Xinlei Chen, Zhuang Liu, In So Kweon, and Saining Xie. Convnext v2: Co-designing and scaling convnets with masked autoencoders. In *Proceedings of the IEEE/CVF Conference on Computer Vision and Pattern Recognition*, pages 16133–16142, 2023. 3
- [40] Lihe Yang, Bingyi Kang, Zilong Huang, Xiaogang Xu, Jiashi Feng, and Hengshuang Zhao. Depth anything: Unleashing the power of large-scale unlabeled data. In *Proceedings of the IEEE/CVF Conference on Computer Vision and Pattern Recognition*, pages 10371–10381, 2024. 3
- [41] Shangzhan Zhang, Sida Peng, Tao Xu, Yuanbo Yang, Tianrun Chen, Nan Xue, Yujun Shen, Hujun Bao, Ruizhen Hu, and Xiaowei Zhou. Mapa: Text-driven photorealistic material painting for 3d shapes. In *ACM SIGGRAPH 2024 Conference Papers*, pages 1–12, 2024. 1, 3, 6
- [42] Xilong Zhou, Milos Hasan, Valentin Deschaintre, Paul Guerrero, Kalyan Sunkavalli, and Nima Khademi Kalantari. Tilegen: Tileable, controllable material generation and capture. In *SIGGRAPH Asia 2022 conference papers*, pages 1–9, 2022. 1
- [43] Xilong Zhou, Milos Hasan, Valentin Deschaintre, Paul Guerrero, Yannick Hold-Geoffroy, Kalyan Sunkavalli, and Nima Khademi Kalantari. Photomat: A material generator learned from single flash photos. In *ACM SIGGRAPH 2023 Conference Proceedings*, pages 1–11, 2023. 1

Harnessing the Power of Foundation Models for Accurate Material Classification

Supplementary Material

6. Class-wise Accuracy on DMS-test

Table 6. reports the per-class classification accuracy on the DMS-test dataset. While Table 2 in the main text only provides the averaged results, this table further breaks down the performance into individual classes. Figure 7 illustrates one representative sample from each of the 21 categories in the DMS-test dataset. The full test set consists of 1,050 images, constructed by retaining connected regions larger than 10,000 pixels in each category and randomly sampling 50 images per category.

Table 6. Comparison with state-of-the-art methods on the DMS-test dataset (21 classes). All values denote classification accuracy (truncated to two decimal places), and the best result in each row is highlighted in **bold**.

Method \ Class	CLIP[29]	GPT-4v [1]	MatSim[9]	Ours
fabric	0.34	0.54	0.28	0.64
foliage	0.60	0.30	0.60	0.74
glass	0.52	0.24	0.16	0.40
leather	0.32	0.42	0.52	0.54
metal	0.32	0.58	0.18	0.82
paper	0.44	0.38	0.36	0.56
plastic	0.24	0.36	0.06	0.74
stone	0.36	0.38	0.20	0.52
water	0.26	0.48	0.38	0.90
wood	0.36	0.80	0.32	0.76
rubber	0.18	0.42	0.30	0.34
ceramic	0.02	0.30	0.40	0.20
sponge	0.32	0.34	0.58	0.66
bone	0.86	0.44	0.58	0.70
cardboard	0.72	0.68	0.42	0.78
concrete	0.22	0.34	0.18	0.56
fur	0.46	0.80	0.58	0.80
gemstone	0.14	0.04	0.66	0.24
soil	0.18	0.30	0.50	0.60
wax	0.50	0.74	0.72	1.00
wicker	0.72	0.36	0.66	0.94
Average	0.38	0.43	0.41	0.64

7. Class-wise Accuracy on Google-test

In addition to the averaged results on the Google-test dataset reported in Table 2 of the main text, we provide a detailed per-class breakdown here. Table 7 presents the class-wise classification accuracy on the Google-test dataset, complementing the averaged results in the main text. This section is parallel to Section 6, which reported the per-class accuracy on the DMS-test dataset. Figure 8 shows selected samples

from the Google-test dataset, in the same manner as Figure 7 for DMS-test. One representative sample is shown for each of the 21 categories. Unlike DMS-test, which was constructed by filtering large connected regions from existing material datasets, Google-test was manually curated from Google Images. It also consists of 21 categories, with 30 images per category, resulting in a total of 630 test images.

Table 7. Comparison with state-of-the-art methods on the Google-test dataset (21 classes). All values denote classification accuracy (truncated to two decimal places), and the best result in each row is highlighted in **bold**.

Method \ Class	CLIP[29]	GPT-4v [1]	MatSim[9]	Ours
fabric	0.33	0.70	0.40	0.83
foliage	1.00	0.50	0.86	1.00
glass	0.83	0.76	0.53	0.90
leather	0.90	1.00	0.66	1.00
metal	0.70	0.60	0.36	1.00
paper	0.76	0.83	0.20	0.86
plastic	0.40	0.96	0.43	0.96
stone	0.83	0.76	0.46	0.96
water	0.86	0.93	0.90	1.00
wood	0.76	0.90	0.60	0.93
rubber	0.50	0.36	0.33	0.53
ceramic	0.56	0.66	0.33	0.70
sponge	1.00	0.90	0.80	0.86
bone	1.00	0.83	0.76	0.93
cardboard	0.93	0.60	0.80	0.96
concrete	0.96	0.90	0.76	0.96
fur	0.83	0.86	0.90	1.00
gemstone	1.00	0.16	0.80	1.00
soil	0.93	0.86	0.66	1.00
wax	1.00	0.86	0.86	1.00
wicker	1.00	0.66	0.86	0.96
Average	0.81	0.74	0.63	0.92

8. Class image statistics

We reported detailed sample statistics for all 21 categories in our own dataset and compared them with the DMS dataset in Table 8. While DMS exhibits significant imbalance across classes, our generative dataset provides a more uniform distribution, enabling better supervision across rare categories.



Figure 7. Illustration of the DMS-test dataset. One representative sample is shown for each of the 21 categories.



Figure 8. Illustration of the Google-test dataset. One representative sample is shown for each of the 21 categories.

9. Samples from our generated dataset

Our generated dataset provides diverse material samples across 21 categories, each accompanied by extracted semantic patches that highlight the fine-grained local cues present in the Figure 9 and Figure 10. These patches capture critical texture, reflectance, and structural details—demonstrating that the synthesized data contains rich and meaningful material semantics suitable for training and analysis.

Table 8. Per-class image statistics for DMS[37] and our synthetic dataset. For each category, the number on the left of “|” denotes the DMS image count, while the number on the right denotes the corresponding count in our synthetic dataset.

Class	DMS[37] Ours	Class	DMS[37] Ours
fabric	31,489 1,345	ceramic	8,314 740
foliage	11,384 1,000	sponge	326 725
glass	28,934 860	bone	3,751 965
leather	7,354 875	cardboard	3,150 1,000
metal	30,504 2,330	concrete	2,853 955
paper	20,763 1,000	fur	1,567 620
plastic	36,937 2,060	gemstone	369 615
stone	4,206 730	soil	1,855 985
water	2,063 1020	wax	1,107 980
wood	26,274 1025	wicker	1,895 1000
rubber	7,811 645		



Figure 9. Samples from our generated dataset and their extracted patches capture local material semantics across 21 classes.



Figure 10. Samples from our generated dataset and their extracted patches capture local material semantics across 21 classes.